ACS APPLIED MATERIALS & INTERFACES

www.acsami.org

Research Article

Monovalent Antigen-Induced Aggregation (MAA) Biosensors Using Immunomagnetic Beads in Both Sample Separation and Signal Generation for Label-Free Detection of Enrofloxacin

Yafang Shen, Fei Jia, Aoming Liang, Yawen He, Yaping Peng, Huang Dai, Yingchun Fu, Jianping Wang,* and Yanbin Li*

Cite This: *ACS Appl. Mater. Interfaces* 2022, 14, 8816−8823

Read Online

ACCESS | Metrics & More | Article Recommendations | Supporting Information

ABSTRACT: Exploring new functions of nanomaterials can help facilitate the development of biosensors for the detection of antibiotics. Herein, a new detection modality based on monovalent antigen-induced aggregation (MAA) of immunomagnetic beads (IMBs) was proposed for rapid and label-free detection of enrofloxacin (ENR), which endowed IMBs with the abilities of both sample separation and signal generation. In the presence of ENR, the initially well-dispersed IMBs were aggregated and the degree of aggregation was in a concentration-dependent manner. After exploring the mechanism underlying IMB aggregation and investigating the key parameters affecting it, a label-free biosensing platform was developed for rapid and sensitive detection of ENR. Based on the significant differences in the magnetic separation speed and size between the aggregated and well-dispersed IMBs, two methods were proposed for quantitatively determining ENR, i.e., measuring the turbidity of the IMB supernatant after magnetic separation for a given time and visualizing and calculating the grayscale value of the aggregated IMBs trapped on the surface of a nitrocellulose membrane. A three-dimensional (3D)-printed syringe was designed and fabricated for automatic filtration of IMBs. This immunosensor allowed for sensitive detection of ENR in less than 15 min without any labels. It exhibited a satisfactory limit of detection of 0.79 ng mL^{-1} and showed the feasibility for ENR detection of spiked chicken meat with recovery rates ranging from 74.8 to 98.3%. The MAA immunosensor can act as a promising tool to detect trace levels of ENR and has the potential to be applied to complex food samples.

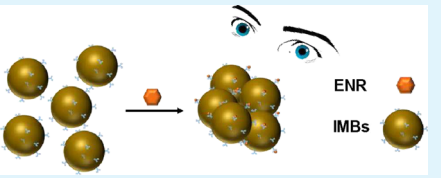

KEYWORDS: *enrofloxacin detection, label-free biosensor, immunomagnetic beads, monovalent antigen-induced aggregation, poultry meat*

INTRODUCTION

Enrofloxacin (ENR) is a major member of the fluoroquinolone family with a broad antimicrobial spectrum against both Gram-positive and Gram-negative bacteria.[1−3] It has been extensively used in poultry and livestock for the treatment and prevention of animal diseases.[4,5] However, the abuse or incorrect use of ENR often results in residues in the environment and food, which may lead to the increased occurrence of resistant bacteria.[6] Consequently, many countries and organizations, including China and the European Union, have set the maximum residue limits (MRLs) for the sum of ENR and ciprofloxacin to 100−300 $\mu g\ kg^{-1}$ in animal tissues (GB 31650-2019; Commission Regulation (EU) No. 37/2010).[7] Conventional methods for ENR detection mainly include chromatographic methods and enzyme-linked immunosorbent assays (ELISA).[8,9] However, they either are sensitive and accurate but require well-trained technicians and expensive apparatus; or are facile and cost-effective but show poor accuracy and stability. Therefore, new methods for rapid, sensitive, and facile detection of ENR are highly in demand.

Biosensors have aroused great interest in the detection of antibiotics owing to their advantages of low cost, high sensitivity, and potential on-site application.[10] Currently, both label-based and label-free modalities have been well developed. Despite showing some advantages on sensitivity and specificity, the label-based methods are not only laborious, time-consuming, and complicated, but additional signal labels may also introduce extra interference and heterogeneity, as well as cost.[11−14] Hence, the development of label-free detection techniques has been stimulated to avoid these drawbacks.

Among various label-free methods, detection strategies based on the aggregation of nanomaterials (e.g., gold nanoparticles (AuNPs), transition-metal dichalcogenide nanosheets, and carbon dots) have drawn increasing attention due to their straightforward signal output and high detection sensitivity.[15−18] Some conventional aggregation-based assays, as represented by the AuNP-based sensors, however, have the disadvantages of nonspecific aggregation and complicated

Received: December 3, 2021
Accepted: January 21, 2022
Published: February 8, 2022

Scheme 1. Illustration of the MAA Immunosensor for ENR Detection with Dual-signal Readout

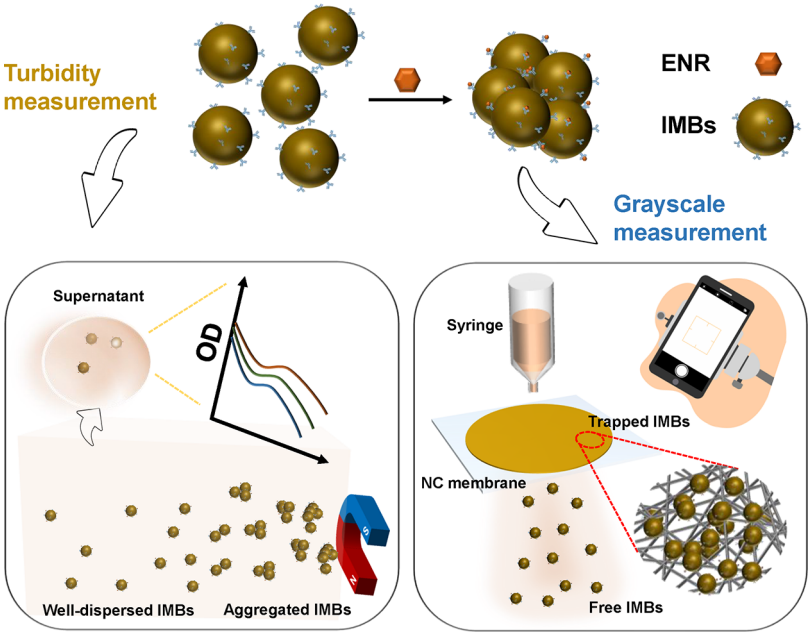

separation/purification, which limit their large-scale in-field applications.[19,20] Therefore, there is still a need for exploring more versatile materials for the fabrication of aggregation-based label-free biosensors.

Magnetic nanoparticles/magnetic beads (MBs) are emerging as promising and intriguing materials in different fields owing to their extraordinary properties of easy manipulation in a magnetic field, satisfactory biocompatibility, large surface area, and accelerated reaction kinetics.[21,22] As commonly used in biosensing applications, MBs play a significant role in the separation, purification, and concentration of targets prior to detection.[23] Despite the fact that most MB-based assays strongly rely on complicated labeling of fluorescent dyes,[24] enzymes,[25] and nanomaterials[26] for signal generation, the label-free detection modalities based on MB aggregation have been proposed, where MBs not only serve as a magnetic separation carrier but also act as a signal generator. Undoubtedly, the integration of magnetic separation with a direct signal output from MBs themselves will greatly simplify the detection procedure, and thus shorten the detection time. In such assays, however, multiple binding sites on an analyte surface are always required for the cross-linking of MBs. Hence, current research on MB aggregation-based assays is mainly restricted to the detection of DNA, bacteria, and biomarkers.[19,27,28] Research on the direct detection of monovalent molecules, such as antibiotics with a limited surface epitope, however, has lagged behind.

In this work, a phenomenon of monovalent antigen-induced aggregation (MAA) of immunomagnetic beads (IMBs) was reported with the exploration of the underlying mechanism, and then a biosensing platform that integrated IMBs for both target separation and signal output was proposed for rapid and facile detection of ENR. As illustrated in Scheme 1, the initially well-dispersed IMBs were aggregated in the presence of ENR. Two different detection strategies, which were based on turbidity and grayscale measurements, respectively, were proposed for signal output. For the former case, IMBs and IMBs−ENR aggregates were magnetically separated for a given period of time, and the turbidity of the collected supernatant was measured for ENR quantitation. For the other, after reacting with ENR, the mixture of IMBs and IMBs−ENR aggregates was loaded into a syringe, then it was dropped and filtered through a nitrocellulose (NC) membrane. Owing to their larger sizes, the aggregated IMBs were trapped on the surface of the NC membrane, while the well-dispersed ones with smaller sizes could pass through the membrane pores easily. The grayscale value of the IMB stain was calculated and correlated to the concentration of ENR using a MATLAB-based program. To the best of our knowledge, this is the first study that utilizes IMB aggregation for direct detection of monovalent molecules without any labels.

MATERIALS AND METHODS

Materials and Apparatus. Carboxyl MBs with diameters of 150 and 100 nm were purchased from Ocean NanoTech, LLC. (San Diego, CA) and Ruixi Biological Technology Co., Ltd. (Xi'an, China), respectively. Monoclonal mouse anti-ENR antibody was purchased from CUSABIO Technology, LLC. (Wuhan, China). *N*-(3-(Dimethylaminopropyl)-*N*′-ethylcarbodiimide hydrochloride (EDC) was bought from Sigma-Aldrich (St. Louis, MO). *N*-Hydroxysulfosuccinimide sodium salt (Sulfo-NHS) and ENR were obtained from Aladdin Chemistry (Shanghai, China). Bovine serum albumin (BSA) was supplied by Sangon Biotech (Shanghai, China). Chloramphenicol (CAP), tetracycline hydrochloride (TET), oxytetracycline hydrochloride (OTC), doxycycline hydrochloride (DOX), and kanamycin sulfate (KAN) obtained from Sangon Biotech (Shanghai, China); ciprofloxacin hydrochloride (CIP) obtained from Aladdin Chemistry (Shanghai, China); and norfloxacin (NOR) and levofloxacin (LEV) purchased from Macklin, Inc. (Shanghai, China) were used as nontargeted antibiotics. An NC membrane with a pore size of 0.45 μm was bought from Watman (Dassel, Germany). All of the other chemicals used in the experiments were of analytical grade or better quality.

The absorbance spectrum was collected using a Synergy H1 Hybrid Multi-Mode Microplate Reader (BioTek Instruments, Winooski, VT) for turbidity measurement. Metallurgical microscopy (MM) images were recorded using a CX40M metallurgical microscope (Sunny Optical Technology, Ningbo, China). ζ Potentials were measured using a Zetasizer Nano ZS-90 (Malvern Instruments, Malvern, UK).

https://doi.org/10.1021/acsami.1c23398
ACS Appl. Mater. Interfaces 2022, 14, 8816−8823

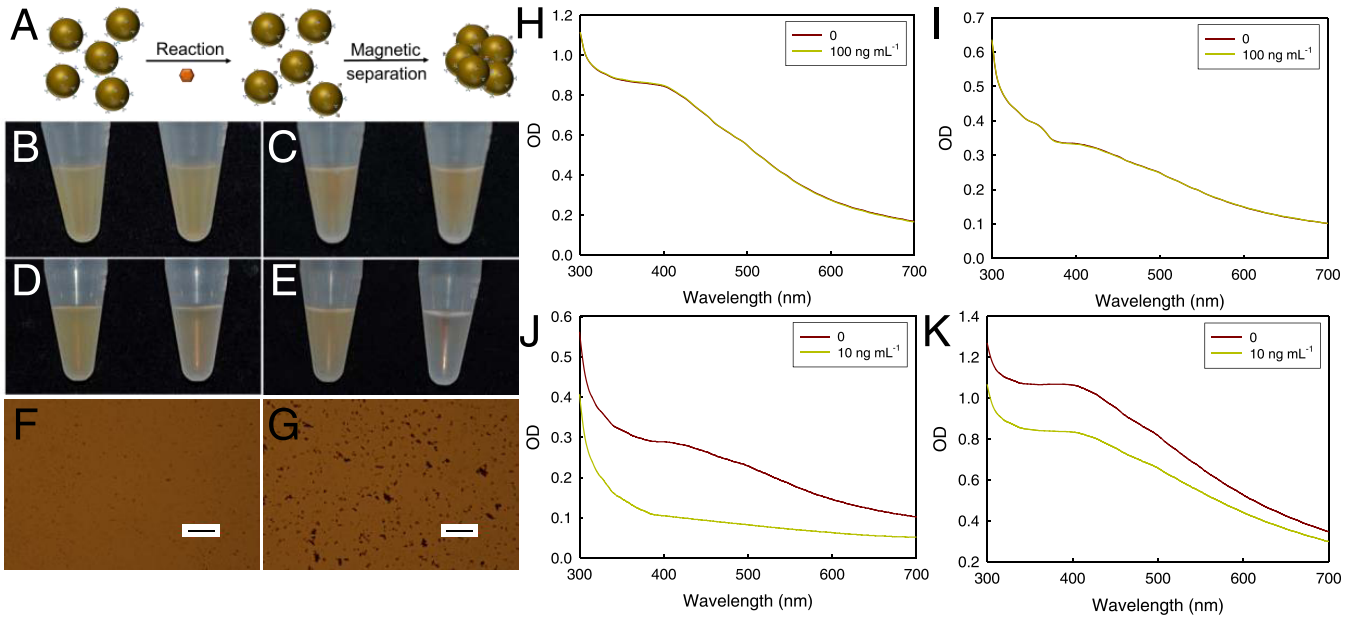

Figure 1. (A) Schematic illustration of IMB aggregation in the presence of ENR. Photographs of IMB solution (B) after immunoreaction, (C) first placed in a magnetic field, (D) resuspension, and (E) then placed in the magnetic field. The left and right tubes (B, C, D, and E) held IMBs in ENR-negative and -positive samples, respectively. MM images of IMBs in (F) ENR-negative and (G) -positive samples. Scale bar = 30 μm. Responses of (H) pristine MBs, (I) BSA-MBs, (J) IMBs, and (K) IMBs* toward ENR.

Deionized water (18.2 MΩ·cm) used throughout the experiment was obtained from a Milli-Q Direct 8 system (Millipore, Bedford, MA).

Preparation of IMBs. IMBs were prepared based on a carbodiimide method referring to our previous work.[29] In brief, 10 μL of carboxyl MBs with a diameter of 150 nm were washed with 2-(*N*-morpholino)ethanesulfonic acid buffer (25 mM, pH 6.0) containing 0.01% Tween-20 three times, resuspended in a mixture of 10 mM EDC and 15 mM Sulfo-NHS, and incubated at room temperature for 30 min to activate the carboxyl groups. The activated beads were collected and washed three times with boric acid-borax buffer (10 mM, pH 7.4) containing 0.01% Tween-20, followed by the addition of 4 μL of antibodies. Then, the mixture was kept stirring for 2.5 h at ambient temperature and incubated with 1% BSA for 1 h to block the unreacted sites. After washing with phosphate-buffered saline (10 mM, pH 7.4) containing 0.01% Tween-20 (PBST) three times, the IMBs were collected, resuspended in 100 μL of PBST, and stored at 4 °C for further use.

Detection of ENR Based on Turbidity Measurements. IMBs (20 μL) were mixed with ENR solution (180 μL) and gently stirred at room temperature for 10 min. After the capture of ENR, the beads were magnetically separated and resuspended in 200 μL of PBST (10 mM, pH 6.0, containing 0.05% Tween-20 and 0.1% BSA). Then the obtained solution was magnetically separated for 20 s, and the supernatant was collected and used for turbidity measurement. The OD value at 400 nm (referred to as OD_{400}) was used for the quantitative detection of ENR.

Detection of ENR Based on Grayscale Measurements. Reaction solution containing free IMBs and IMBs−ENR composites were obtained via the same procedure as described previously. After magnetic separation, the beads were resuspended in 100 μL of PBST. The solution (50 μL) was loaded into a three-dimensional (3D)-printed syringe and filtered through an NC membrane. The aggregated IMBs−ENR composites with larger sizes were trapped on the surface of the NC membrane, while the free ones with smaller sizes passed through membrane pores more easily, leading to a color difference after drying when IMBs were incubated with different concentrations of ENR. The grayscale value of the IMBs stain was calculated using a MATLAB-based program for ENR detection.

Detection of ENR in Spiked Chicken Meat. The chicken meat was pretreated referring to our previous work with some modifications.[29] The chicken breast was minced and homogenized. Three grams of the homogenate was spiked by spraying different concentrations of ENR and then incubated at ambient temperature for 2 h, followed by the addition of 5.4 mL of 2% 5-sulfosalicylic acid solution. The mixture was ultrasonically treated for 15 min for ENR extraction. Afterward, the liquid was filtered through membranes with pore sizes of 0.45 μm and 0.22 μm successively. After dilution to 10-fold, 180 μL of the extracts were used for ENR detection.

Statistical Analysis. Means and standard deviations were calculated using Microsoft Excel 2010 (Microsoft Corp., Redmond, WA). Significance analysis was performed by the analysis of variance (ANOVA) with a statistical significance threshold of $P < 0.05$.

RESULTS AND DISCUSSION

Mechanism of ENR-Induced IMB Aggregation. ENR solution was mixed with IMBs in a fixed time (10 min in this study). In the absence of ENR, IMBs were well-dispersed during the process of magnetic separation and resuspension; in contrast, though no obvious aggregation was observed after immunoreaction, the presence of ENR induced the formation of large aggregates after magnetic separation, and the aggregates could be separated very quickly when placed in a magnetic field again (Figure 1A−E). MM images also revealed apparent IMB aggregation in the presence of ENR with the aggregate size reaching micrometer levels (Figure 1F,G). This phenomenon was interesting and the underlying mechanism was explored.

As is well known, the magnetic separation efficiency of magnetic particles can be improved by increasing the particle size.[30] Meanwhile, the absorbance of IMB solution increased accordingly with the increase of IMB concentrations (Figure S1). Hence, the absorbance spectra (or OD_{400} value) of the supernatant after magnetic separation for a given time were used to describe the degree of IMB aggregation. A decline in the absorbance/OD_{400} value suggested a higher degree of IMB aggregation.

The aggregation of IMBs was understood to proceed via the reaction between ENR and IMBs where MBs acted as a solid

https://doi.org/10.1021/acsami.1c23398
ACS Appl. Mater. Interfaces 2022, 14, 8816−8823

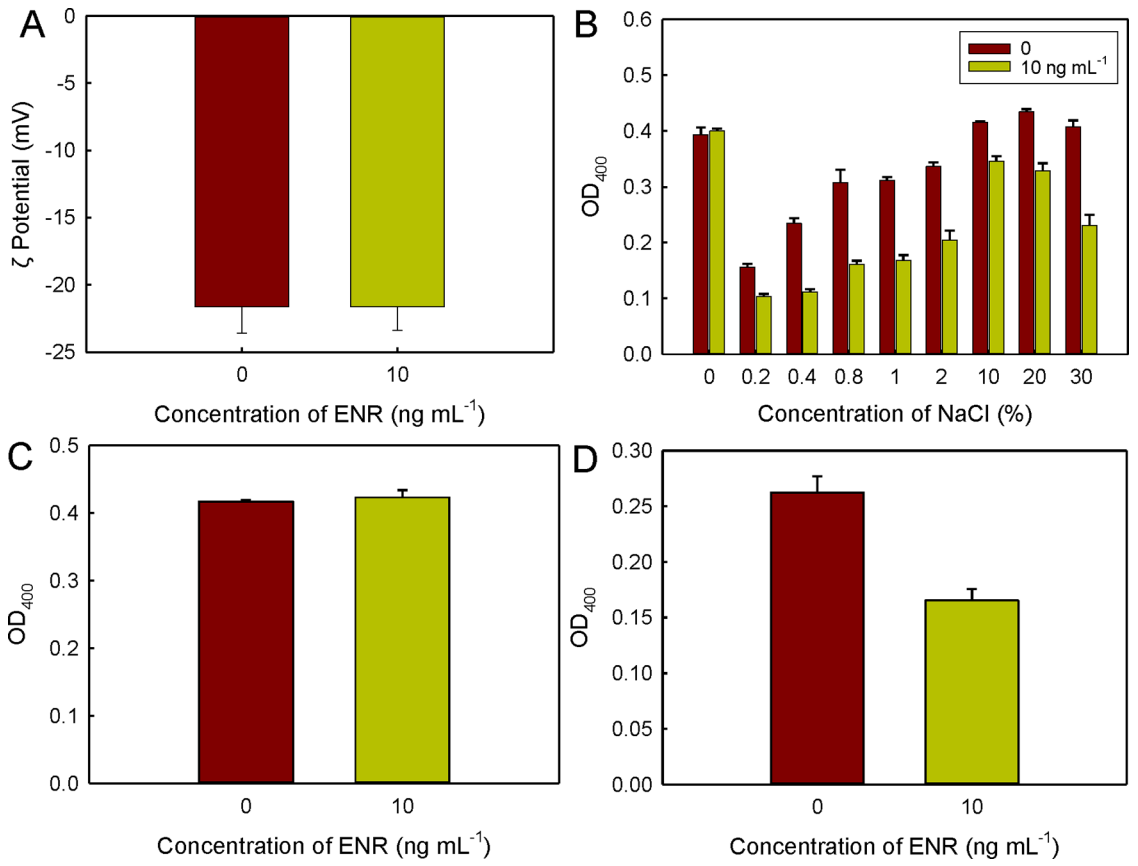

Figure 2. (A) ζ Potentials of IMBs in ENR-negative and -positive samples. (B) Effect of the sodium chloride concentration on MAA. (C) OD_{400} value of the IMB supernatant after the immunoreaction but without the assistance of magnetic force. (D) OD_{400} value of the IMB supernatant with the assistance of centrifugal force.

carrier, BSA as a blocking agent and the immobilized antibodies were possible reaction participants. In separate experiments, ENR was mixed with pristine carboxyl MBs, BSA-modified MBs (BSA-MBs), and antibody-modified MBs in which the MBs were different in surface modification and diameters (IMBs for MBs with a diameter of 150 nm and IMBs* for MBs with a diameter of 100 nm). As shown in Figure 1H−K, ENR-induced aggregation appeared only in IMBs and IMBs*, revealing the key role of antibodies. Therefore, IMB aggregation was proved to be a result of the specific antigen−antibody immunoreaction.

Considering the important role of surface charge played on colloidal stability,[31] the ζ potentials of IMBs and IMBs−ENR composites were measured. As shown in Figure 2A, there was no significant difference between the two groups (−21.6 ± 1.96 mV for IMBs and −21.6 ± 1.77 mV for IMBs−ENR composites, $P > 0.05$), excluding the obvious change of surface charge after the immunoreaction. Therefore, the surface charge may not be the reason for the ENR-induced IMB aggregation.

Following tests indicated that sodium chloride played an important role in the IMB aggregation (Figure 2B). Moreover, with low sodium chloride concentrations, both IMBs and IMBs−ENR composites were poorly suspended. Interestingly, a non-Derjaguin−Landau−Verwey−Overbeek (non-DLVO) behavior was observed at higher sodium chloride concentrations. This "anomalous" restabilization has been observed in antibody-coated latex microspheres and other protein latex complexes which can be explained by the hydration force.[32−34] Hydration force becomes significant for a more hydrophilic surface.[32] Therefore, the free energy of the system increases with the decrease of surface hydrophilicity. Compared to ENR-free samples, the trends of IMB aggregation were always higher after reaction with ENR. Considering the significant role of hydrophobic interactions played in antibody recognition and antigen−antibody immunoreaction,[35] we hypothesized that the binding of ENR increased the hydrophobicity of the IMB surface, which in turn decreased the hydration force and increased the hydrophobic force, and thus induced the aggregation. A similar phenomenon was also observed in the presence of some other electrolytes except for magnesium chloride (Figure S2) because Mg^{2+} belongs to chaotropic ions that may shield the hydrophobic interaction.[36,37]

Furthermore, IMB aggregation appeared only with the assistance of magnetic force. Without preseparation under a magnetic field, there was no obvious difference in the aggregation states between IMBs and IMBs−ENR composites (Figure 2C). Other external forces such as centrifugal force also induced similar aggregation (Figure 2D). This is similar to hydrophobic shear flocculation where mechanical conditioning is necessary for overcoming the energy barrier.[30] Particle hydrophobicity plays an important role in shear flocculation,[38] which further supports our hypothesis.

The aforementioned results indicated that the aggregation of IMBs after reaction with ENR was likely driven by the increased hydrophobicity on the IMB surface upon ENR binding. The increased hydrophobicity can be explained by (1) the exposure of hydrophobic regions after the antigen−

https://doi.org/10.1021/acsami.1c23398
ACS Appl. Mater. Interfaces 2022, 14, 8816−8823

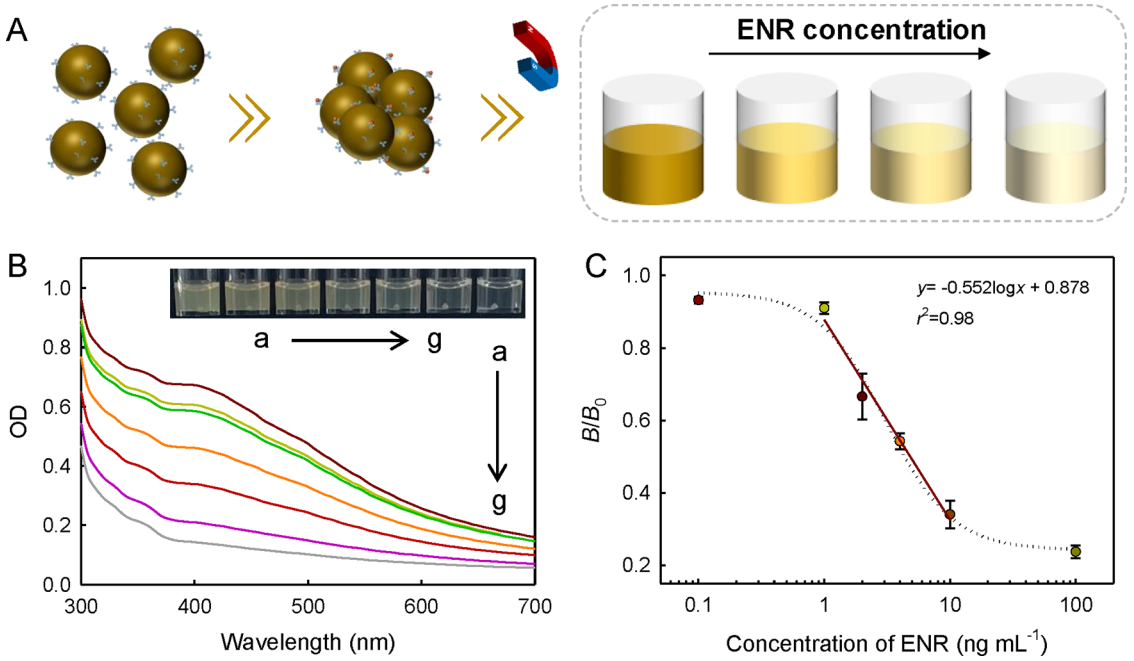

Figure 3. (A) Schematic illustration of ENR detection based on turbidity measurements. (B) Absorbance spectra of the IMB supernatant with different ENR concentrations and the corresponding images. The concentrations of ENR were 0, 0.1, 1, 2, 4, 10, and 100 ng mL^{-1} (from a to g). (C) The relationship between B/B_0 and the logarithm of the ENR concentration. The dotted and solid lines represent the fitted curve in the whole investigated concentration range and the calibration curve in the linear detection range, respectively.

antibody reaction and (2) the high hydrophobicity of ENR molecules.

ENR Detection Based on Turbidity Measurements. As mentioned, IMBs aggregated in the presence of ENR. It showed great potential to be developed into a biosensor for label-free detection of ENR. Since the aggregates were separated very quickly in an applied magnetic field, turbidity measurement of the supernatant after magnetic separation was utilized for the quantitative detection of ENR (Figure 3A). First, major experimental variables including the concentration of IMBs, reaction time, and pH were optimized (Table S1).

Under the optimized conditions, the performance of the turbidity measurement-based biosensor was investigated. With the increase of the ENR concentration, the absorbance of the IMB supernatant decreased accordingly (Figure 3B). As shown in Figure 3C, the signal responses B/B_0 ($B = OD_{400}$ value at a concentration of ENR and $B_0 = OD_{400}$ value in the absence of ENR) against the logarithm of ENR concentrations could be fitted using a four-parameter logistic model. It exhibited a linear detection range from 1 to 10 ng mL^{-1}, and the regression equation was $y = -0.552 \log x + 0.878$ ($r^2 = 0.98$), where y and x represent B/B_0 and the concentration of ENR, respectively. The limit of detection (LOD), defined as the concentration which is corresponding to three times the standard deviations below the mean of the signals of the negative control, was calculated to be 0.79 ng mL^{-1}. Compared to other reported methods for ENR detection, it can be found that the proposed method showed superiority in rapidity (less than 15 min) without the compromise of sensitivity (Table S2).

ENR Detection Based on Grayscale Measurements. Compared to well-dispersed IMBs, the aggregated ones are larger in size, making them more difficult to penetrate through a membrane. Therefore, the degree of IMB aggregation was assumed to be determined by measuring the color of IMBs remaining on the surface of the membrane after filtration (Figure 4A).

To verify the concept, vacuum filtration of IMBs after reaction with ENR was conducted. As shown in Figure 4B, compared with the well-dispersed IMBs in a negative sample, the aggregated ones displayed a darker stain on an NC membrane, indicating that more IMBs were trapped on the surface. Moreover, IMB stains on the reverse side and a second layer of the membrane were also observed. As expected, the positive sample showed lighter stains both on the reverse side and the second layer because fewer IMBs would pass through the NC membrane. These revealed the feasibility of the filtration method for ENR detection.

Inspired by commercial syringe filters that consist of a syringe for liquid pumping and a membrane serving as a filter, a simple 3D-printed device for automatic IMB filtration was designed and fabricated in our laboratory on the basis of a commercial low-cost and disposable syringe. Figure 4C shows the conceptual design, section diagram, and photographs of the device where a spring was attached to the end of a 3D-printed plunger to automatically expel the IMB solution inside. And a circular nozzle was installed in the head of the syringe for sample loading and control of the shape of the stains. Under the action of the spring, IMB solution can be expelled and filtered through the NC membrane automatically. Afterward, the resulting IMB stains were photographed using a smartphone and processed in a MATLAB-based program for grayscale value calculation.

As a proof-of-concept, ENR with different concentrations in PBST was tested. As shown in Figure 4D, the grayscale values decreased obviously with the increase of ENR concentrations, and a linear relationship was established between the grayscale value (y) and the logarithm of the ENR concentration (x) which could be described as $y = -8.515 \log x + 178.169$ ($r^2 = 0.993$) with a LOD of 7.77 ng mL^{-1}. Compared with turbidity

https://doi.org/10.1021/acsami.1c23398
ACS Appl. Mater. Interfaces 2022, 14, 8816−8823

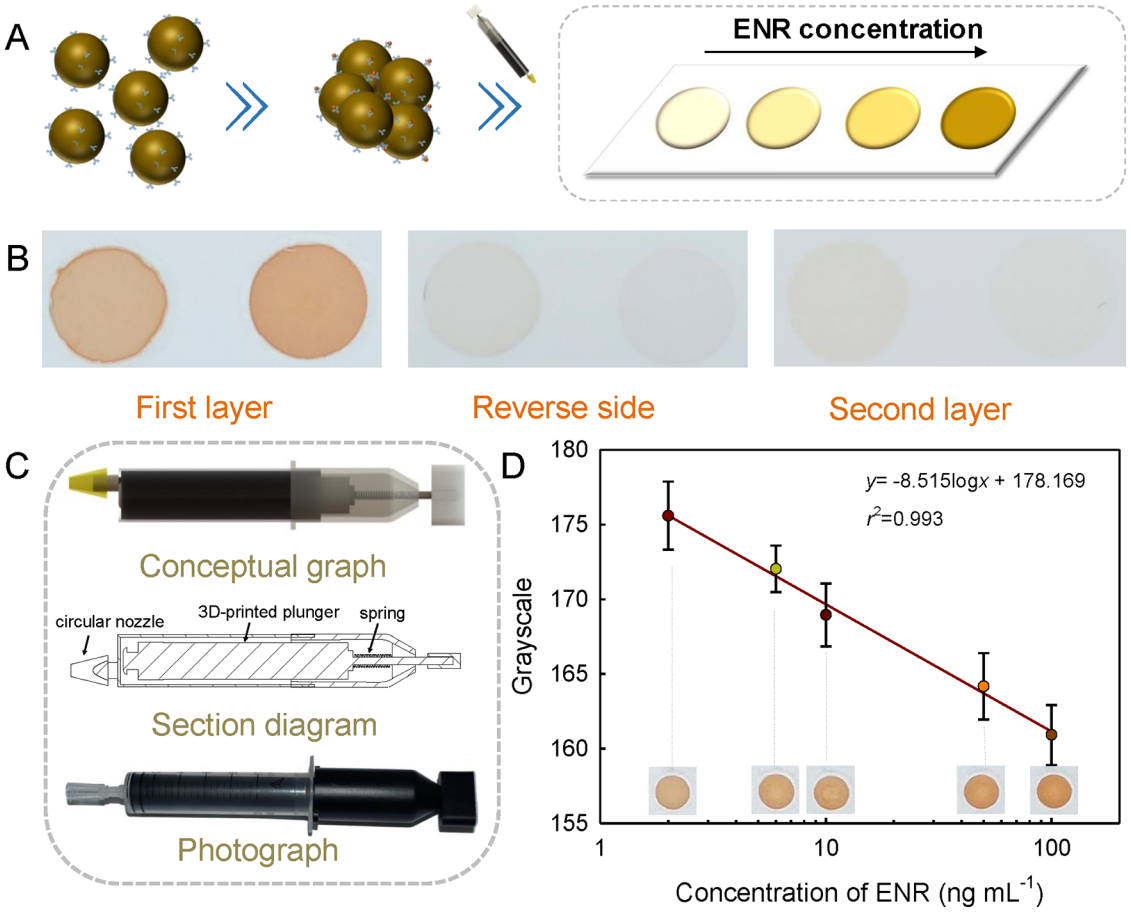

Figure 4. (A) Schematic illustration of ENR detection based on grayscale measurements. (B) Photographs of IMB stains on the first layer, reverse side, and second layer of the NC membrane. The left and right stains were IMBs in ENR-negative and -positive samples, respectively. (C) Conceptual graph, section diagram, and photographs of the 3D-printed syringe. (D) The linear relationship between the grayscale value and the logarithm of ENR concentration and corresponding images. The concentrations of ENR were 2, 6, 10, 50, and 100 ng mL^{-1}.

measurements, the grayscale measurement-based method is less sensitive with a higher LOD (approximately 10-fold). However, it avoids the requirement of any sophisticated apparatus, showing the great potential of in-field applications.

Specificity of the Assay. To determine the specificity of the proposed biosensor, LEV, NOR, and CIP that belong to the family of fluoroquinolones, and other kinds of antibiotics, OTC, TET, DOX, CAP, and KAN at a concentration of 10 ng mL^{-1} were tested. Compared to the negative control, CAP, LEV, DOX, KAN, TET, and OTC showed no significant difference ($P > 0.05$), while CIP, NOR, and ENR were significantly different ($P < 0.001$) (Figure 5). The results revealed that the developed immunosensor displayed negligible cross-reactivity to other groups of antibiotics, but had cross-reactivity to CIP and NOR. The cross-reactivity is ascribed to the structural similarity of these fluoroquinolone antibiotics. As shown in Figure S3, ENR, CIP, and NOR possess high molecular structure similarities. In addition to the basic quinolone structure, they all contain a piperazinyl ring and an alkyl group at position 7 and position 1, respectively,[39] leading to the high cross-reactivity of the produced antibodies toward these three antibiotics. When compared with CIP and NOR, the biosensor was more sensitive to ENR since the decline of the OD_{400} value in the presence of ENR reached 65%, which was significantly different from CIP (41%) or NOR (45%). Meanwhile, the cross-reactivity of the biosensor

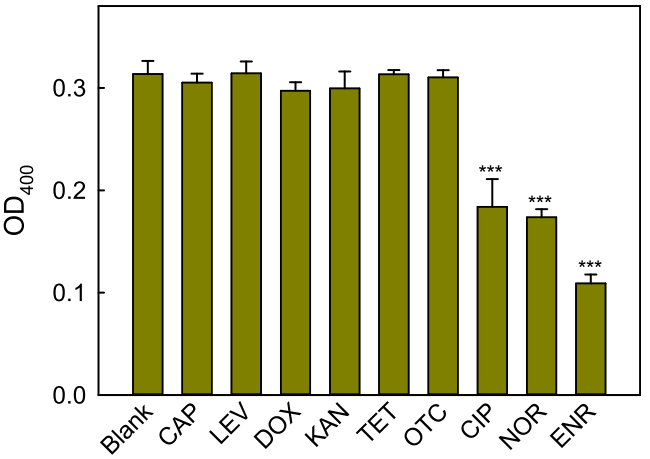

Figure 5. OD_{400} value of the IMB supernatant after reaction with different antibiotics. Asterisks indicated a significant difference in the OD_{400} values between the negative control and antibiotic samples. Statistical analysis was performed using ANOVA followed by post hoc multiple comparisons using Dunnett's test.

to another fluoroquinolone antibiotic LEV was negligible. LEV also contains the piperazinyl ring at position 7, however, it possesses a six-membered ring around positions 1 and 8.[40] Therefore, LEV appears more different from ENR, CIP, and NOR, which may result in negligible reactivity.

https://doi.org/10.1021/acsami.1c23398
ACS Appl. Mater. Interfaces 2022, 14, 8816−8823

Detection of ENR in Spiked Chicken Meat. To evaluate the feasibility of the biosensor for detection of ENR in actual samples, ENR spiked in chicken meat was detected. First, a calibration curve was established for the quantitative detection of ENR in chicken meat (Figure S4) with a linear detection range of 20−1000 $\mu g\ kg^{-1}$ and a LOD of 18.5 $\mu g\ kg^{-1}$. The calculated LOD was below the MRLs of ENR in chicken muscle (100 $\mu g\ kg^{-1}$), as regulated by China and the European Union. Then, spiked chicken meat with ENR concentrations of 25, 100, and 150 $\mu g\ kg^{-1}$ were detected. The average recovery rates ranged from 74.8 to 98.3% (Table 1). Hence, the developed immunosensor is feasible for ENR detection in complex chicken meat.

Table 1. Recovery Rates of ENR in Chicken Meat (n = 3)

spiked ($\mu g\ kg^{-1}$)	detected ($\mu g\ kg^{-1}$)	recovery rate (%)
25	18.7 ± 2.7	74.8
100	86.1 ± 9.1	86.1
150	147.4 ± 20.2	98.3

CONCLUSIONS

In this study, a new biosensing modality based on MAA was exploited for rapid and label-free detection of ENR. The aggregation of IMBs may turn out to be a result of the increased hydrophobicity of the IMB surface after ENR binding. Two biosensing strategies based on the changes in magnetic separation speed and size were proposed for ENR detection. A 3D-printed syringe was designed and fabricated for automatic filtration of IMBs. The LOD for ENR was down to 0.79 ng mL^{-1}, which was better than or comparable to most immunoassays with complicated signal generation/amplification. And the detection could be finished within 15 min which was superior to most analogues. This method integrated IMBs for both separation/purification and signal generation, which had the potential of rapid, label-free, portable, and in-field detection of ENR residues in the food supply chain. Because IMB aggregation induced by a monovalent antigen depends largely on surface properties, future work may focus on the mechanism of interactions between target molecules and their corresponding antibodies to improve the universality of this method.

ASSOCIATED CONTENT

Supporting Information

The Supporting Information is available free of charge at https://pubs.acs.org/doi/10.1021/acsami.1c23398.

Absorbance of IMB solution with different concentrations; effect of other electrolytes on ENR detection; molecular structures of ENR, CIP, NOR, and LEV; calibration curve for ENR detection in spiked chicken meat; optimization of the experimental parameters; comparison of the performance of different methods for ENR detection (PDF)

AUTHOR INFORMATION

Corresponding Authors

Jianping Wang − *College of Biosystems Engineering and Food Science, Zhejiang University, Hangzhou 310058, China;* orcid.org/0000-0002-2551-4564; Email: jpwang@zju.edu.cn

Yanbin Li − *Department of Biological and Agricultural Engineering, University of Arkansas, Fayetteville, Arkansas 72701, United States;* orcid.org/0000-0002-4142-7743; Email: yanbinli@uark.edu

Authors

Yafang Shen − *College of Biosystems Engineering and Food Science, Zhejiang University, Hangzhou 310058, China*

Fei Jia − *College of Biosystems Engineering and Food Science, Zhejiang University, Hangzhou 310058, China*

Aoming Liang − *College of Biosystems Engineering and Food Science, Zhejiang University, Hangzhou 310058, China*

Yawen He − *College of Biosystems Engineering and Food Science, Zhejiang University, Hangzhou 310058, China*

Yaping Peng − *College of Biosystems Engineering and Food Science, Zhejiang University, Hangzhou 310058, China*

Huang Dai − *College of Food Science and Engineering, Wuhan Polytechnic University, Wuhan 430023, China*

Yingchun Fu − *College of Biosystems Engineering and Food Science, Zhejiang University, Hangzhou 310058, China;* orcid.org/0000-0003-0550-9052

Complete contact information is available at: https://pubs.acs.org/10.1021/acsami.1c23398

Author Contributions

The manuscript was written through contributions of all authors. All authors have given approval to the final version of the manuscript.

Notes

The authors declare no competing financial interest.

ACKNOWLEDGMENTS

This research was funded in part by the National Natural Science Foundation of China (32102058), the Walmart Foundation (project # 0402-70013-21-0000), and the China Postdoctoral Science Foundation (2020M681867), and supported by the Walmart Food Safety Collaboration Center.

REFERENCES

(1) Tian, R.; Ji, J.; Zhou, Y.; Du, Y.; Bian, X.; Zhu, F.; Liu, G.; Deng, S.; Wan, Y.; Yan, J. Terminal-Conjugated Non-Aggregated Constraints of Gold Nanoparticles on Lateral Flow Strips for Mobile Phone Readouts of Enrofloxacin. *Biosens. Bioelectron.* **2020**, *160*, No. 112218.

(2) Rezende, J. d. P.; Pacheco, A. F. C.; Magalhães, O. F.; Coelho, Y. L.; Vidigal, M. C. T. R.; da Silva, L. H. M.; Pires, A. C. d. S. Polydiacetylene/Triblock Copolymer/Surfactant Nanoblend: A Simple and Rapid Method for the Colorimetric Screening of Enrofloxacin Residue. *Food Chem.* **2019**, *280*, 1−7.

(3) Xu, Y.; Jiang, D.; Zhang, M.; Zhang, Z.; Qian, J.; Hao, N.; Ding, C.; Wang, K. High-Performance Photoelectrochemical Aptasensor for Enrofloxacin Based on Bi-Doped Ultrathin Polymeric Carbon Nitride Nanocomposites with SPR Effect and Carbon Vacancies. *Sens. Actuators, B* **2020**, *316*, No. 128142.

(4) Aymard, C.; Kanso, H.; Serrano, M. J.; Pagan, R.; Noguer, T.; Istamboulie, G. Development of a New Dual Electrochemical Immunosensor for a Rapid and Sensitive Detection of Enrofloxacin in Meat Samples. *Food Chem.* **2021**, *370*, No. 131016.

(5) Sanllorente, S.; Rubio, L.; Ortiz, M. C.; Sarabia, L. A. Signal Transfer with Excitation-Emission Matrices Between a Portable Fluorimeter Based on Light-Emitting Diodes and a Master Fluorimeter. *Sens. Actuators, B* **2019**, *285*, 240−247.

(6) Song, Y.; Xu, M.; Liu, X.; Li, Z.; Wang, C.; Jia, Q.; Zhang, Z.; Du, M. A Label-Free Enrofloxacin Electrochemical Aptasensor

Constructed by a Semiconducting CoNi-Based Metal-Organic Framework (MOF). *Electrochim. Acta* **2021**, *368*, No. 137609.
(7) Hong, J.; Liu, X.; Yang, X.; Wang, Y.; Zhao, L. Ionic Liquid-Based Dispersive Liquid−Liquid Microextraction Followed by Magnetic Solid-Phase Extraction for Determination of Quinolones. *Microchim. Acta* **2022**, *189*, No. 8.
(8) Wang, R.; Li, S.; Chen, D.; Zhao, Y.; Wu, Y.; Qi, K. Selective Extraction and Enhanced-Sensitivity Detection of Fluoroquinolones in Swine Body Fluids by Liquid Chromatography−High Resolution Mass Spectrometry: Application in Long-Term Monitoring in Livestock. *Food Chem.* **2021**, *341*, No. 128269.
(9) Tufa, R. A.; Pinacho, D. G.; Pascual, N.; Granados, M.; Companyó, R.; Marco, M. P. Development and Validation of an Enzyme Linked Immunosorbent Assay for Fluoroquinolones in Animal Feeds. *Food Control* **2015**, *57*, 195−201.
(10) Majdinasab, M.; Mishra, R. K.; Tang, X.; Marty, J. L. Detection of Antibiotics in Food: New Achievements in the Development of Biosensors. *TrAC, Trends Anal. Chem.* **2020**, *127*, No. 115883.
(11) Chaudhuri, S.; Korten, T.; Korten, S.; Milani, G.; Lana, T.; te Kronnie, G.; Diez, S. Label-Free Detection of Microvesicles and Proteins by the Bundling of Gliding Microtubules. *Nano Lett.* **2018**, *18*, 117−123.
(12) Hai, X.; Li, Y.; Zhu, C.; Song, W.; Cao, J.; Bi, S. DNA-Based Label-Free Electrochemical Biosensors: From Principles to Applications. *TrAC, Trends Anal. Chem.* **2020**, *133*, No. 116098.
(13) Leung, C.-H.; Wu, K.-J.; Li, G.; Wu, C.; Ko, C.-N.; Ma, D.-L. Application of Label-Free Techniques in Microfluidic for Biomolecules Detection and Circulating Tumor Cells Analysis. *TrAC, Trends Anal. Chem.* **2019**, *117*, 78−83.
(14) Xu, M.; Wang, R.; Li, Y. Electrochemical Biosensors for Rapid Detection of *Escherichia coli* O157:H7. *Talanta* **2017**, *162*, 511−522.
(15) Lan, L.; Yao, Y.; Ping, J.; Ying, Y. Ultrathin Transition-Metal Dichalcogenide Nanosheet-Based Colorimetric Sensor for Sensitive and Label-Free Detection of DNA. *Sens. Actuators, B* **2019**, *290*, 565−572.
(16) Peng, H.; Chen, I. A. Rapid Colorimetric Detection of Bacterial Species Through the Capture of Gold Nanoparticles by Chimeric Phages. *ACS Nano* **2019**, *13*, 1244−1252.
(17) Hu, S.; Huang, P.-J. J.; Wang, J.; Liu, J. Dissecting the Effect of Salt for More Sensitive Label-Free Colorimetric Detection of DNA Using Gold Nanoparticles. *Anal. Chem.* **2020**, *92*, 13354−13360.
(18) Bhatt, M.; Bhatt, S.; Vyas, G.; Raval, I. H.; Haldar, S.; Paul, P. Water-Dispersible Fluorescent Carbon Dots as Bioimaging Agents and Probes for Hg^{2+} and Cu^{2+} Ions. *ACS Appl. Nano Mater.* **2020**, *3*, 7096−7104.
(19) Chen, Y. P.; Xianyu, Y. L.; Sun, J. S.; Niu, Y. J.; Wang, Y.; Jiang, X. Y. One-Step Detection of Pathogens and Cancer Biomarkers by the Naked Eye Based on Aggregation of Immunomagnetic Beads. *Nanoscale* **2016**, *8*, 1100−1107.
(20) Xianyu, Y.; Lin, Y.; Chen, Q.; Belessiotis, A.; Stevens, M.; Thomas, M. Iodide-Mediated Rapid and Sensitive Surface Etching of Gold Nanostars for Biosensing. *Angew. Chem., Int. Ed.* **2021**, *60*, 9891−9896.
(21) Shen, Y.; Xu, L.; Li, Y. Biosensors for Rapid Detection of *Salmonella* in Food: A Review. *Compr. Rev. Food Sci. Food Saf.* **2021**, *20*, 149−197.
(22) Wang, L.; Lin, J. Recent Advances on Magnetic Nanobead Based Biosensors: From Separation to Detection. *TrAC, Trends Anal. Chem.* **2020**, *128*, No. 115915.
(23) Zhu, W.; Chen, Y.; He, Y.; Fang, W.; Ying, Y.; Li, Y.; Fu, Y. Cooperation Mode of Outer Surface and Inner Space of Nanochannel: Separation-Detection System Based on Integrated Nanochannel Electrode for Rapid and Facile Detection of *Salmonella*. *Anal. Chem.* **2020**, *92*, 1818−1825.
(24) Liu, X.; Liao, X.; Jia, B.; Sun, C.; Zhou, L.; Kong, W. Development of a Multi-Channel Magnetic Bead Micro-Probe Assay for High-Throughput Detection of Zearalenone in Edible and Medicinal Coix Seed. *Food Chem.* **2021**, *347*, No. 128977.
(25) Wang, X.; Cohen, L.; Wang, J.; Walt, D. R. Competitive Immunoassays for the Detection of Small Molecules Using Single Molecule Arrays. *J. Am. Chem. Soc.* **2018**, *140*, 18132−18139.
(26) Wang, L.; Hao, L.; Qi, W.; Huo, X.; Xue, L.; Liu, Y.; Zhang, Q.; Lin, J. A Sensitive *Salmonella* Biosensor Using Platinum Nanoparticle Loaded Manganese Dioxide Nanoflowers and Thin-Film Pressure Detector. *Sens. Actuators, B* **2020**, *321*, No. 128616.
(27) Roy, S.; Abd Rahman, I.; Ahmed, M. U. Paper-Based Rapid Detection of Pork and Chicken Using LAMP-Magnetic Bead Aggregates. *Anal. Methods* **2016**, *8*, 2391−2399.
(28) Leslie, D. C.; Li, J.; Strachan, B. C.; Begley, M. R.; Finkler, D.; Bazydlo, L. A. L.; Barker, N. S.; Haverstick, D. M.; Utz, M.; Landers, J. P. New Detection Modality for Label-Free Quantification of DNA in Biological Samples via Superparamagnetic Bead Aggregation. *J. Am. Chem. Soc.* **2012**, *134*, 5689−5696.
(29) Shen, Y.; He, Y.; Fu, Y.; Wang, J.; Zhang, J.; Liao, M.; Li, Y. A Nanomaterial-Based Biosensor for the Quantitative Detection of Enrofloxacin Residues in Raw Chicken. *Trans. ASABE* **2020**, *63*, 1869−1878.
(30) Song, S.; Lu, S.; Lopez-Valdivieso, A. Magnetic Separation of Hematite and Limonite Fines as Hydrophobic Flocs from Iron Ores. *Miner. Eng.* **2002**, *15*, 415−422.
(31) Bozó, T.; Mészáros, T.; Mihály, J.; Bóta, A.; Kellermayer, M. S. Z.; Szebeni, J.; Kálmán, B. Aggregation of PEGylated Liposomes Driven by Hydrophobic Forces. *Colloids Surf., B* **2016**, *147*, 467−474.
(32) Dávalos-Pantoja, L.; Ortega-Vinuesa, J. L.; Bastos-Gonzalez, D.; Hidalgo-Alvarez, R. Colloidal Stability of IgG- and IgY-Coated Latex Microspheres. *Colloids Surf., B* **2001**, *20*, 165−175.
(33) López-León, T.; Jodar-Reyes, A. B.; Ortega-Vinuesa, J. L.; Bastos-Gonzalez, D. Hofmeister Effiects on the Colloidal Stability of an IgG-Coated Polystyrene Latex. *J. Colloid Interface Sci.* **2005**, *284*, 139−148.
(34) Molina-Bolivar, J. A.; Galisteo-Gonzalez, F.; Hidalgo-Alvarez, R. Stabilization of Protein-Latex Complexes at High Ionic Strength. *Colloids Surf., B* **1996**, *8*, 73−80.
(35) Yuan, M.; Na, Y.; Li, L.; Liu, B.; Sheng, W.; Lu, X.; Kennedy, I.; Crossan, A.; Wang, S. Computer-Aided Molecular Modeling Study on Antibody Recognition of Small Molecules: An Immunoassay for Triazine Herbicides. *J. Agric. Food Chem.* **2012**, *60*, 10486−10493.
(36) Baca, M.; De Vos, J.; Bruylants, G.; Bartik, K.; Liu, X.; Cook, K.; Eeltink, S. A Comprehensive Study to Protein Retention in Hydrophobic Interaction Chromatography. *J. Chromatogr. B* **2016**, *1032*, 182−188.
(37) Löwenberg, C.; Julich-Gruner, K. K.; Neffe, A. T.; Behl, M.; Lendlein, A. Salt-Induced Shape-Memory Effect in Gelatin-Based Hydrogels. *Biomacromolecules* **2020**, *21*, 2024−2031.
(38) Akdemir, Ü.; Hicyilmaz, C. Shear Flocculation of Chromite Fines in Sodium Oleate Solutions. *Colloids Surf., A* **1996**, *110*, 87−93.
(39) Wang, Z.; Zhu, Y.; Ding, S.; He, F.; Beier, R. C.; Li, J.; Jiang, H.; Feng, C.; Wan, Y.; Zhang, S.; Kai, Z.; Yang, X.; Shen, J. Development of a Monoclonal Antibody-Based Broad-Specificity ELISA for Fluoroquinolone Antibiotics in Foods and Molecular Modeling Studies of Cross-Reactive Compounds. *Anal. Chem.* **2007**, *79*, 4471−4483.
(40) Cao, L.; Kong, D.; Sui, J.; Jiang, T.; Li, Z.; Ma, L.; Lin, H. Broad-Specific Antibodies for a Generic Immunoassay of Quinolone: Development of a Molecular Model for Selection of Haptens Based on Molecular Field-Overlapping. *Anal. Chem.* **2009**, *81*, 3246−3251.

https://doi.org/10.1021/acsami.1c23398
ACS Appl. Mater. Interfaces 2022, 14, 8816−8823